

Feedback control of a magnetic bearing using fusion of rotor acceleration and position measurements

Matthew O T Cole^a, Samuel Jimenez^a, Patrick S Keogh^a

^a Department of Mechanical Engineering, University of Bath, Bath BA2 7AY, UK, m.o.t.cole@bath.ac.uk

Abstract—This paper considers controlling a magnetic bearing using combined feedback of rotor acceleration and position measurements. A controller design based on sensor fusion via complementary filtering is described. The control method can maintain stability while allowing the cross-over frequency for the acceleration and position feedback loops to be set arbitrarily. In this way, position measurements can be utilized primarily for disturbance cancellation over a low frequency band while acceleration feedback maintains bearing stability and disturbance rejection over a higher frequency band. The approach has the advantage that it gives enhanced robustness to poor quality position measurements. For flexible rotors, stabilization with large axial separation of position sensors and bearing locations can be easily achieved by utilizing collocated rotor-embedded accelerometers. The approach also offers improved robustness to measurement noise, position sensor run-out error and other forms of physical contamination or damage. Through analysis and simulation, important physical effects on vibration control performance are identified and further considered within the design methodology.

I. INTRODUCTION

The use of rotor-embedded sensors in combination with high-speed wireless transmission holds significant promise for application to condition monitoring and vibration control of rotating machines. This paper considers the utilization of acceleration sensors fixed within a rotor in combination with external position sensing as a means to stabilize and control a magnetic bearing. A potential advantage of using acceleration sensors is a low vulnerability to physical damage, debris contamination and run-out errors that can adversely affect the operation of noncontact displacement sensors such as eddy current probes. The ability to obtain vibration measurements at locations that are inaccessible to externally mounted probes may also be important. The possibility of using additional accelerometer-based feedback to stabilize a system with very low bandwidth position sensors provides further motivation for this study. In this respect, the technique has relevance to, and may be useful in combination with, self-sensing magnetic bearings [1-4].

Sensor data-fusion is important for various motion control/tracking applications where there is no single reliable means to obtain absolute position information [5-8].

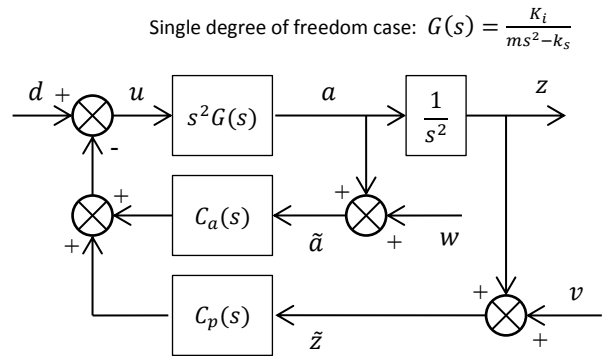


Figure 1. Combined acceleration-position feedback control of a rotor-AMB system.

Controllers for large-gap magnetic levitation systems have also been developed via this approach [9]. The successful utilization of rotor-mounted accelerometers, however, presents some unique challenges. This preliminary work shows that a given controller designed for position feedback stabilization can be used within a control strategy based on complementary filtering of acceleration and position measurements. In this way direct forcing disturbance rejection characteristics can be set according to a prototype feedback controller design. Sensitivity to measurement error, noise or other disturbances can be independently adjusted through a frequency domain weighting of sensor signals, chosen according to anticipated spectral characteristics of disturbances.

II. HYBRID ACCELERATION-POSITION FEEDBACK CONTROL

A. Complementary filter design

A parallel feedback of acceleration and position measurements to control a rotor-AMB system may be considered as shown in Fig. 1. The transfer function $G(s)$ represents the open loop dynamics from AMB control currents to rotor displacements z . Measurement of acceleration a is subject to an additive disturbance w , while the disturbance v acts additively on the displacement measurements. For illustration purposes, a single-degree-of-freedom (1-DOF) lumped-mass model may be considered (with G as in Fig. 1).

Formulation of a sensor-fusion strategy can be based on an arbitrary pair of complementary filters with transfer functions $F_1(s)$ and $F_2(s)$ satisfying

$$F_1 + F_2 = 1 \quad (1)$$

For the control structure shown in Fig. 1, a prototype stabilizing controller H may be included in the feedback path transfer functions according to

$$C_p = F_1 H, \quad C_a = \frac{F_2 H}{s^2} \quad (2)$$

The closed loop transfer functions relating the rotor displacement to each disturbance signal are then given by

$$T_{zd} = \frac{G}{1 + GH}, T_{zv} = \frac{F_1 GH}{1 + GH}, T_{zw} = \frac{F_2 GH}{s^2(1 + GH)} \quad (3)$$

Stabilization and direct disturbance rejection characteristics, as determined by T_{zd} , can be assigned through standard design procedures for the controller H . Separately, the characteristics of T_{zv} and T_{zw} , which dictate sensor noise/disturbance sensitivity, can be balanced through an appropriate choice of F_1 (and F_2). Clearly, for position feedback only, $F_1 = 1$ and $F_2 = 0$. With combined feedback, the complementary filters can be chosen so that C_p and C_a both have low-pass characteristics, thereby achieving insensitivity to noise and other forms of zero-mean measurement error. Care must be taken within the design process to consider offset errors, particularly due to gravitational effects, that might affect acceleration measurements and result in a large or unbounded displacement response. Such instability is associated with zero-valued poles of T_{zw} and, in general, can be overcome by ensuring F_2 has a sufficient number of zero-valued zeros.

For illustration, consider a prototype design for H based on a standard PID control law:

$$H = K_I/s + K_P + K_D s \quad (4)$$

Complementary filters could be synthesized according to optimal estimation methods, typically in the form of an extended Kalman filter [6,7]. However, this approach requires stochastic information on expected measurement disturbances. In the absence of such information, a generic low-pass/high-pass filter pair may be considered:

$$F_1 = \frac{(s+\omega_c)^{N-s^N}}{(s+\omega_c)^N}, \quad F_2 = \frac{s^N}{(s+\omega_c)^N} \quad (5)$$

This leads to

$$C_p = \frac{((s+\omega_c)^{N-s^N})(K_I+K_P s+K_D s^2)}{s(s+\omega_c)^N} \quad (6)$$

$$C_a = \frac{K_I+K_P s+K_D s^2}{s^{3-N}(s+\omega_c)^N} \quad (7)$$

Note that the cross-over frequency $\omega_c > 0$ directly determines the high frequency gain of C_p (as given by $\omega_c K_D$) and can be chosen arbitrarily small.

It follows from (3) that

$$T_{zw} = \frac{K_I+K_P s+K_D s^2}{(s+\omega_c)^N} \cdot \frac{G s^{N-2}}{(s+G(K_I+K_P s+K_D s^2))} \quad (8)$$

Examining the multiplicity of zero-valued zeros of T_{yw} indicates that, to eliminate steady-state displacement error subject to constant offset in the acceleration measurement, requires $N \geq 3$. A further conclusion here is that the use of

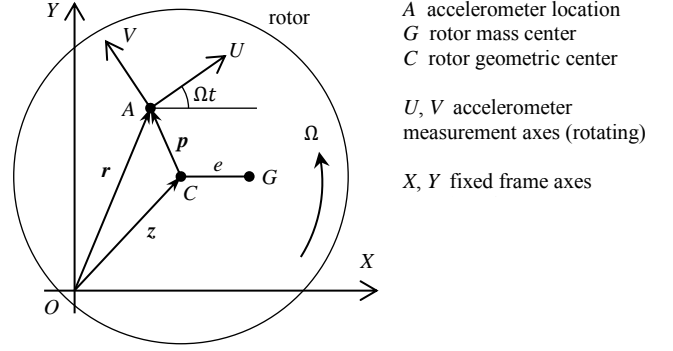


Figure 2. Geometry of rotor acceleration measurements

acceleration signals alone ($N = 0$) will not achieve stabilization.

B. Rotational effects

For control of a spinning rotor using measurements of acceleration at points fixed within the rotor, consideration must be given to:

- The effect of accelerometer rotation and positioning eccentricity with respect to geometric and inertial centres of the rotor.
- The effect of gravity on measurements by the accelerometer.
- Possible non-collocation of position and acceleration sensors.

Measurements from accelerometers will relate to fixed-frame motion of the rotor according to the geometry shown in Fig. 2. Suppose that a two-axis accelerometer is positioned internally to the rotor at point A and has orthogonal sensing axes (U, V) lying within the plane of rotation. The position of point A relative to the origin of the fixed frame is

$$\mathbf{r} = \mathbf{z} + \mathbf{p} \quad (9)$$

where \mathbf{z} is the position vector for the rotor center, as would be measured by rotor displacement sensors. For conciseness, complex notation is adopted: $\mathbf{r} = r_x + jr_y$. The corresponding vector in the rotating frame is $\bar{\mathbf{r}} = \mathbf{r} e^{-j\Omega t} = r_u + jr_v$. Accordingly, $\mathbf{p} = \bar{\mathbf{p}} e^{j\Omega t}$ where $\bar{\mathbf{p}}$ is a constant vector defining the accelerometer position relative to the rotor center. Therefore, the accelerometer eccentricity can be denoted $|\mathbf{p}|$. It follows that,

$$\dot{\mathbf{r}} = \dot{\mathbf{z}} - \Omega^2 \bar{\mathbf{p}} e^{j\Omega t} \quad (10)$$

An acceleration measurement in the non-rotating frame (including gravity effects) at point A would be

$$\tilde{\mathbf{a}} = \dot{\mathbf{z}} - \Omega^2 \bar{\mathbf{p}} e^{j\Omega t} + jg \quad (11)$$

where the last two terms are considered as error terms. The actual measurements by the accelerometer a_u, a_v are given by

$$a_u + ja_v = \tilde{\mathbf{a}} e^{-j\Omega t} = \dot{\mathbf{z}} e^{-j\Omega t} - \Omega^2 \bar{\mathbf{p}} + jg e^{-j\Omega t} \quad (12)$$

The error component from centrifugal acceleration $-\Omega^2 \bar{\mathbf{p}}$ acts in an unchanging direction but increases in magnitude with rotational speed. Although this component could be estimated and compensated for within a control implementation, care must still be taken to ensure it does not cause saturation problems.

The acceleration measurements are also contaminated by a synchronously rotating gravity component. Although various

TABLE I. PARAMETERS FOR ROTOR-AMB SIMULATION MODEL

Parameter	Value
m	Rotor mass 10 Kg
R	Rotor diameter (in sensor plane) 0.03 m
k_s	AMB negative stiffness 0.3×10^6 N/m
K_i	AMB current gain 97.5 N/A
$K_I K_i$	Net integral gain 100 Nm/s
$K_P K_i$	Net proportional gain 1×10^6 N/m
$K_D K_i$	Net derivative gain 1000 Ns/m

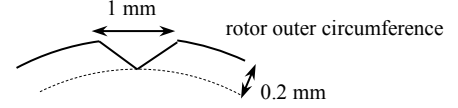


Figure 3. Geometry of run-out error used for simulations. This example case could represent circumferential damage to the rotor at the displacement sensor location, e.g. due to impact

methods to compensate for this component could be envisaged, inexact cancellation will lead to stability/drift problems, as discussed in Section II.A. Addressing this issue within the complementary filter design is therefore desirable.

To use the measured accelerations for control, a counter-rotating transformation can be applied to recover the fixed-frame acceleration signal prior to feedback. Complementary filtering can then be applied as described in Section II.A. Filtering could alternatively be applied in the co-rotating (accelerometer) frame rather than the stationary frame. A combination of filtering in both frames may also be possible and could help to eliminate both static and synchronous disturbance components from measurement/ response signals.

III. RESPONSE BEHAVIOUR

In this section of the paper the influence of filtering on vibration response and error sensitivity are investigated through time-step simulation of a linearized 2-DOF rotor-

AMB model with the parameters detailed in Table I. The results presented in Fig. 4 involve a supercritical rotational speed of 400 rad/s. The three cases simulated correspond to three different complementary filter designs. In all cases, the underlying controller is PID type with parameter values given in Table I. All three simulation runs involve the same set of disturbance conditions. Initially, the rotor is well-balanced and vibration is induced only by the effect of centrifugal acceleration at the accelerometer location, which acts through the control feedback path. The accelerometer eccentricity is $|p| = 0.1$ mm. After 0.3 seconds, a rotor unbalance condition is instantaneously introduced resulting in an increase in vibration in all three cases. The eccentricity of the rotor center of mass is $e = 0.1$ mm. After 0.6 seconds a run-out error is further introduced affecting the position measurement according to the geometry shown in Fig. 3.

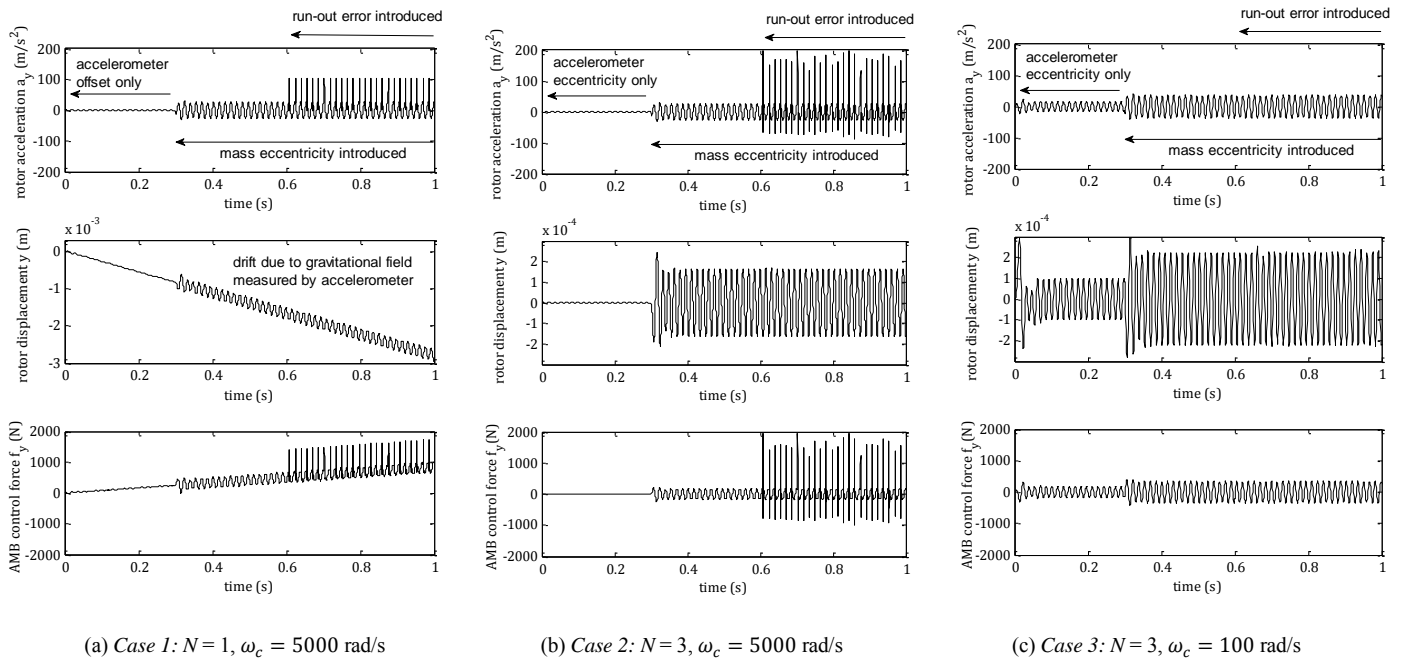


Figure 4. Simulated rotor-AMB behaviour under combined acceleration-position feedback. System model and controller parameters are given in Table I. Rotational speed $\Omega = 400$ rad/s. Rotor unbalance (mass-eccentricity of 1×10^{-3} kg-m) is introduced after 0.3 seconds and run-out error introduced after 0.6 seconds. Results are shown for three different complementary filters designs.

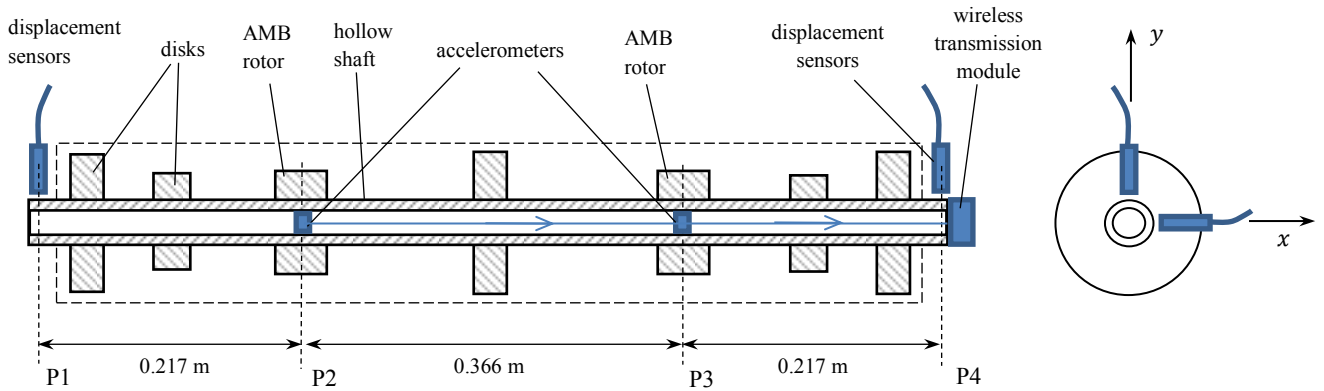


Figure 5. Layout of hollow-shaft flexible rotor system with position sensing in planes P1, P4 and acceleration sensing in planes P2, P3 collocated with AMBs

Some important features of the response behaviour can be identified from the simulation results. For Case 1, the complementary filter is a first order design ($N = 1$). Although the rotor acceleration seems well-controlled, the displacement of the rotor drifts in an unstable manner. This is caused by offset in the fixed-frame acceleration signal due to gravity, as discussed in Section II. Use of a third order complementary filter design ($N = 3$) overcomes this problem, as seen in Case 2. Rotor acceleration measurements are similar to the first case but unstable drift of rotor position is prevented. For Cases 1 and 2, the cross-over frequency for the complementary filter design is $\omega_c = 5000$ rad/s and so the rotor is predominantly position-controlled over the frequency range of the disturbances. Introducing the run-out error shown in Fig. 3 causes large spikes in the rotor acceleration due to the action of the feedback control. Correspondingly, large spikes can be seen in the AMB control signal. Associated issues with vibration/noise transmission and force saturation would be expected. Case 3 involves the same 3rd order complementary filter design but with a lower cross-over frequency of $\omega_c = 100$ rad/s. In this case, position errors introduced by the run-out damage are effectively filtered by the position feedback loop such that control forces and rotor accelerations are unaffected. As a further observation, the rotor vibration response due to unbalance is the same in all three cases. This can be explained by the fact that the transfer function T_{zd} is independent of the filter transfer functions F_1 and F_2 .

IV. FLEXIBLE ROTOR TEST SYSTEM

A numerical study on the application of the proposed approach to a fully levitated flexible rotor test system (Fig. 5) has been undertaken. The system has a hollow shaft rotor that is 0.8 m in length and 0.03 m in diameter. A number of disks are mounted along the rotor at the positions indicated in Fig. 5. The natural frequencies and mode shapes of the first three flexural modes of the free rotor are shown in Fig. 6. The nominal rotational speed range of 0-12000 rpm (0-1260 rad/s) covers the critical speed associated with the first flexural mode only. The characteristics of the AMBs match those given in Table I for the 1-DOF system.

The main focus of this study is the effect of non-collocation of position sensors and AMBs. A hybrid sensor configuration, as shown in Fig. 5, is of practical interest as it would separate all sensors from working sections of the rotor, thus protecting sensors from unfavorable environmental conditions such as high temperatures, direct contact with pumped/working fluids or contaminants. It could also lower the risk of debris or impact related damage and allow easy servicing and replacement. Nonetheless, for the sensor configuration shown in Fig. 5, use of either displacement or acceleration sensors alone would present difficulties in achieving stable levitation. For position-based feedback alone, the large axial separation of the displacement sensors and AMBs would necessitate model-based controller design to stabilize flexural modes, with stringent requirements on robustness to model-error. For acceleration-feedback control, collocation of accelerometers and magnetic bearings can be exploited by a passivity-based controller design (including modified PD controllers). However, stable drift-free levitation is unachievable with acceleration feedback alone. By combining sensor information using a MIMO version of the complementary filtering approach described in Section II, stable levitation and satisfactory vibration attenuation performance can be achieved with model-free controller designs.

To analyze achievable control performance, a rotordynamic model based on finite element methods has been constructed. Details on such methods and the conversion to standard first order state-space form can be found elsewhere [10, 11]. To construct an appropriate model of the complete system, the relation between lateral force

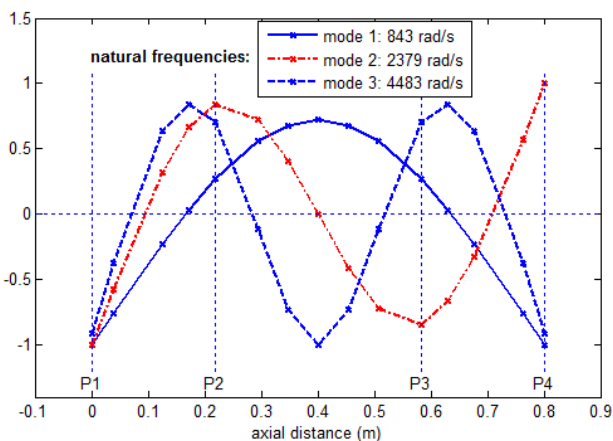


Figure 6. Natural frequencies and mode shapes for first three flexural modes of the free rotor

components $\mathbf{f}_m = [f_x, f_y]$ applied to the rotor in plane m and the rotor displacement response $\mathbf{z}_n = [x, y]$ in plane n is considered in the standard form

$$\dot{\mathbf{x}} = \mathbf{A}\mathbf{x} + \mathbf{B}_m\mathbf{f}_m \quad (13)$$

$$\mathbf{z}_n = \mathbf{C}_n\mathbf{x} \quad (14)$$

The rotor acceleration in plane n is

$$\mathbf{a}_n = \ddot{\mathbf{z}}_n = \mathbf{C}_n\dot{\mathbf{x}} = \mathbf{C}_n\mathbf{A}^2\mathbf{x} + \mathbf{C}_n\mathbf{A}\mathbf{B}_m\mathbf{f}_m \quad (15)$$

The MIMO transfer function for the open loop system, combining four displacement measurements in planes 1 and 4 and four acceleration measurements in planes 2 and 3, is

$$\mathbf{C}(\mathbf{I}s - \mathbf{A})^{-1}\mathbf{B} + \mathbf{D} = \begin{bmatrix} \mathbf{C}_{1,4} \\ \mathbf{C}_{2,3}\mathbf{A}^2 \end{bmatrix} (\mathbf{I}s - \mathbf{A})^{-1} \mathbf{B}_{2,3} + \begin{bmatrix} \mathbf{0} \\ \mathbf{C}_{2,3}\mathbf{A}\mathbf{B}_{2,3} \end{bmatrix} \quad (16)$$

The controller transfer function is assigned as

$$\mathbf{C}_c(\mathbf{I}s - \mathbf{A}_c)^{-1}\mathbf{B}_c + \mathbf{D}_c = \begin{bmatrix} F_1H & 0 & 0 & 0 & F_2H/s^2 & 0 & 0 & 0 \\ 0 & F_1H & 0 & 0 & 0 & F_2H/s^2 & 0 & 0 \\ 0 & 0 & F_1H & 0 & 0 & 0 & F_2H/s^2 & 0 \\ 0 & 0 & 0 & F_1H & 0 & 0 & 0 & F_2H/s^2 \end{bmatrix} \quad (17)$$

A prototype PID feedback controller H was selected with the gain values given in Table 1. With standard collocated position-based feedback, the closed loop sensitivity function T_{z_v} has the form shown in Fig. 7, which is within ISO recommended limits for AMB control [12]. The complementary filters were selected according to (5) with $N = 3$. The closed loop transfer functions under hybrid feedback defined by (16) and (17) can be computed as

$$\begin{bmatrix} T_{zd}(s) \\ T_{zw}(s) \end{bmatrix} = \begin{bmatrix} \mathbf{C}_z(\mathbf{I}s - \mathbf{A}_{cl})^{-1}\mathbf{B}_d \\ \mathbf{C}_z(\mathbf{I}s - \mathbf{A}_{cl})^{-1}\mathbf{B}_w \end{bmatrix} \quad (18)$$

where

$$\mathbf{A}_{cl} = \begin{bmatrix} \mathbf{A} + \mathbf{B}\mathbf{D}_c\mathbf{C} & \mathbf{B}\mathbf{C}_c \\ \mathbf{C}\mathbf{B}_c & \mathbf{A}_c + \mathbf{B}_c\mathbf{D}_c\mathbf{C}_c \end{bmatrix},$$

$$\mathbf{C}_z = \begin{bmatrix} \mathbf{C}_{1,4} & \mathbf{0} \end{bmatrix}, \quad \mathbf{B}_d = \begin{bmatrix} \mathbf{B}_{2,3} \\ \mathbf{B}_c\mathbf{D} \end{bmatrix}, \quad \mathbf{B}_w = \begin{bmatrix} \mathbf{B}_{2,3}\mathbf{D}_c \\ \mathbf{B}_c \end{bmatrix} \times \begin{bmatrix} \mathbf{0} \\ \mathbf{I} \end{bmatrix}$$

From the closed loop model (18) a parametric study on the influence of filter cross-over frequency ω_c on control performance may be undertaken. Figure 7 showing a map of how the natural frequencies and stability properties of closed loop eigenmodes (as calculated from \mathbf{A}_{cl}) vary with ω_c . For large ω_c , the AMBs are predominantly position-controlled over the frequency range covering the first three flexural modes. Due to the non-collocation of planes P1 and P4 with planes P2 and P3 and phasing associated with the mode shapes (Fig. 6), all three modes are unstable. As ω_c is decreased the flexural modes are sequentially stabilized, until for $\omega_c < 120$ rad/s the closed loop system is stabilized.

Selection of an appropriate value of ω_c should also take into account the frequency domain properties of T_{zd} and T_{zw} , i.e. the rotor displacement response due to direct forcing and accelerometer measurement noise, respectively. For illustration, the maximum singular values of $T_{zd}(j\omega)$ and $T_{zw}(j\omega)$ are shown in Fig. 9 for three different values of ω_c . For $\omega_c \rightarrow 0$, the dynamic properties of T_{zd} tend to replicate

those for the prototype (collocated position-based feedback) design. However, the down side of this is an increased sensitivity to low frequency noise affecting accelerometer measurements. As low frequency noise and drift can be a significant problem for conventional accelerometer designs, there is clearly a compromise to be made in this respect. Further theoretical work is recommended to fully investigate the performance trade-offs inherent in the proposed feedback control approach. It is anticipated that consideration of stochastic (or deterministic) information for expected sensor error/noise and disturbances should provide a systematic approach to shape the stability and response characteristics under combined acceleration and position feedback control. Comparisons with model-based optimal controller design methods would also be worthwhile.

V. WIRELESS SENSING IMPLEMENTATION

For practical implementation of the proposed rotor acceleration feedback, rotor-embedded sensors must satisfy requirements of compact size, high resolution and bandwidth, low noise and straightforward integration with wireless technology. Practical work has focused on combining MEMS digital accelerometers with a microcontroller and wireless radio module for data transmission (Arduino Mini with ATmega328 processor and XBee 802.15.4 wireless module). The accelerometer is a 3-axis device with $\pm 16g$ measurement range and 13 bit resolution, giving a sensitivity of 4mg/LSB. It can provide up to 3.2 kHz sampling rate, measures $3 \times 3 \times 1$ mm and can withstand accelerations up to 10,000 g. These devices work with low supply voltages (2.6V) and have low power consumption so that battery supply or inductive transmission of power are both viable. The microcontroller (with clock speed of 2 MHz) is sufficiently powerful to manage data transfer between multiple accelerometers and the wireless module. Based on four measurement channels, each with sampling frequency of 3.2 kHz, a radio transmission rate > 1 Mbits/s is considered adequate. For

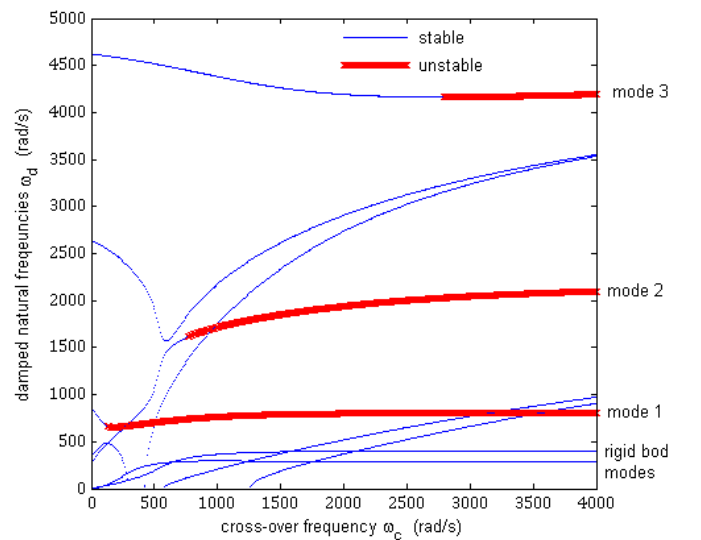


Figure 7. Map showing how the natural frequencies and stability properties of closed loop eigenmodes vary with cross-over frequency for complementary filtering

short range transmission, Wireless USB or Bluetooth 3.0 are suitable protocols. Testing of open-loop data acquisition under rotating conditions has confirmed viability of the approach and further work is in progress to realize full multi-sensor closed loop control.

VI. CONCLUSIONS

An investigation on the control of a rotor-AMB system using combined feedback of rotor acceleration and position measurements has been undertaken. A complementary filtering has been described that can maintain stability while allowing the cross-over frequency for the position and acceleration feedback loops to be freely chosen. The potential advantage of this approach in respect of achieving improved robustness to position sensor run-out error was demonstrated in simulation. Further investigations on the application of the method to model-free control of a multi-mode flexible rotor system have been undertaken. The potential to maintain control stability and vibration attenuation performance with large axial separation of position sensors and AMBs has been shown. Practical realizations will open up new possibilities for AMB-rotor design topologies, free of the limitations imposed by conventional proximity-based collocated sensing of rotor outer surfaces.

REFERENCES

- [1] D. Atsumo, T. Yoshida, K. Ohniwa, "Sensorless control of axial magnetic bearings", *IEEJ Transactions on Industry Applications*, vol. 130, no. 6, pp. 826-827, 2010.
- [2] R. Herzog, S. Vuilloud, R. Amstad, G. Galdos, P. Muellhaupt, R. Longchamp "Self-sensing of non-laminated axial magnetic bearings: modelling and validation", *Proceedings of 11th Int. Symp. Magnetic Bearings*, pp.575-581, pp. 2008
- [3] E. H. Maslen, D. T. Montie, T. Iwasaki, "Robustness limitations in self-sensing magnetic bearings", *Journal of Dynamic Systems, Measurement and Control, Transactions of the ASME*, vol. 128, no. 2, pp. 197-203, 2006.
- [4] G. Van Schoor, A.C. Niemann, C.P. Du Rand, "Evaluation of demodulation algorithms for robust self-sensing active magnetic bearings", *Sensors and Actuators, A: Physical*, vol. 189, pp. 441-450, 2013.
- [5] D. Gruyer, A. Lambert, M. Perrollaz, D. Gingras, "Experimental comparison of Bayesian positioning methods based on multi-sensor data fusion", *International Journal of Vehicle Autonomous Systems*, vol. 12, no. 1, pp. 24-43, 2014.

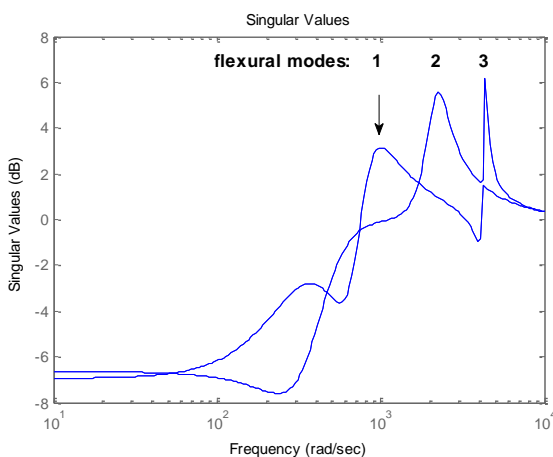
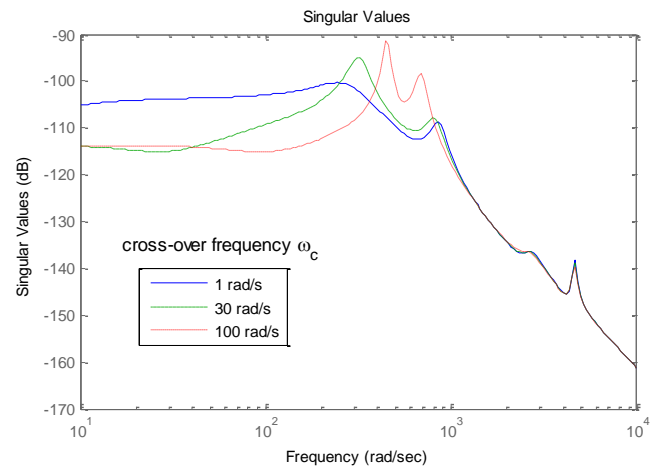
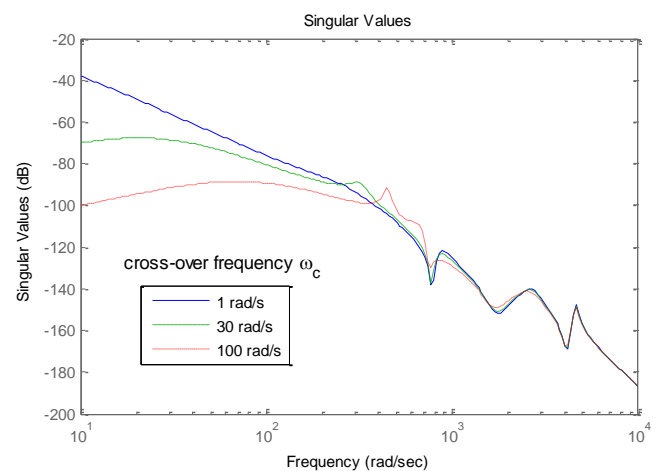


Figure 8. Sensitivity function T_{zv} for prototype feedback controller H designed for feedback of collocated rotor displacement measurements

- [6] H. Zhao, Z. Wang, "Motion measurement using inertial sensors, ultrasonic sensors, and magnetometers with extended Kalman filter for data fusion", *IEEE Sensors Journal*, vol. 12, no. 5, pp. 943-953, 2012.
- [7] I. A. Mahmood, S.O.R. Moheimani, K. Liu, "Tracking control of a nanopositioner using complementary sensors", *IEEE Transactions on Nanotechnology*, vol. 8, no. 1, pp. 55-65, 2009.
- [8] K. K. Tan, P.V. Er, R. Yang, C. S. Teo, "Selective precision motion control using weighted sensor fusion approach", *Proceedings of IEEE International Conference on Mechatronics and Automation*, pp. 179-184, 2013.
- [9] P. J. Berkelman, R. L. Hollis, S.E. Salcudean, "Interacting with virtual environments using a magnetic levitation haptic interface" *Proceedings of IEEE International Conference on Intelligent Robots and Systems*, vol. 1, pp. 117-122, 1995.
- [10] Zorzi, E.S. and Nelson, H.D., Finite-element simulation of rotor-bearing systems with internal damping. *Journal of Engineering for Power-Transactions of the Asme*. vol. 99. No. 1, pp. 71-76, 1977.
- [11] G. Schweitzer, E. Maslen (Eds.), *Magnetic Bearings - Theory, Design, and Application to Rotating Machinery*, Springer, ISBN 978-3-642-00496-4.
- [12] ISO TC108/SC2 Working Group 7. *Active magnetic bearings - evaluation of stability margin*. ISO-14839-3, September 2006.



(a) Direct forcing disturbance sensitivity T_{zd}



(b) Accelerometer noise sensitivity T_{zw}

Figure 9. Frequency response plots showing influence of filter cross-over frequency on disturbance rejection characteristics